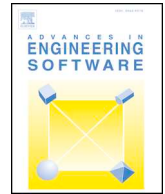




ELSEVIER

Contents lists available at ScienceDirect

Advances in Engineering Software

journal homepage: www.elsevier.com/locate/advengsoft

Research paper

Linked simulation for fire-exposed elements using CFD and thermo-mechanical models

Stanislav Šulc^{*,a}, Vit Šmilauer^a, Bořek Patzák^a, Kamila Cábová^b, František Wald^b^a Faculty of Civil Engineering, Department of Mechanics, Czech Technical University in Prague, Thákurova 7, 166 29 Prague 6, Czech Republic^b Faculty of Civil Engineering, Department of Steel and Timber Structures, Czech Technical University in Prague, Thákurova 7, 166 29 Prague 6, Czech Republic

ARTICLE INFO

Keywords:

CFD
Fire
Fire dynamics simulator
OOFEM
MuPIF
Linking
Adiabatic surface temperature

ABSTRACT

Structural fire assessment belongs essentially to the design of steel, concrete or timber structures. The article presents a weakly-linked computational approach, employing the concept of adiabatic surface temperature (AST). The simulation comprises computational fluid dynamics (CFD), heat transport and solid mechanics. Application programming interfaces in linked codes (FDS, OOFEM) define methods for steering, data storage, visualization or fields mapping. The linked simulation is successfully validated on timber and concrete structural elements exposed to fire.

1. Introduction

The fire resistance of structures relies, to a large extent, on prescriptive-based international codes and standards such as IBC, NBCC, Eurocode, CSA, ASTM, or AISC [8]. The majority of them define time-dependent temperature curves which are used in the design, estimation of fire resistance and also for testing structural elements in furnaces. Such a pragmatic approach offers several benefits, however, it may suffer in unknown joint details, large deformations, new materials, complex geometries, or the assessment of structural reliability. In addition, performance-based design can define further objectives for fire extent, innovative design solutions, a prolonged fire resistance period or increased reliability [12].

Numerical models address the above-mentioned objectives to a large extent. Computational fluid dynamics (CFD) brings solutions of Navier-Stokes equations, supplemented often with mass and species transport. The Fire Dynamics Simulator (FDS) represents such a widely-used, open source code, which was developed at NIST [16]. The code has been validated on a variety of simulation scenarios [1,15,18].

A weak and discretized form of heat balance and equilibrium equations provides the framework for thermo-mechanical analysis using the finite element method (FEM) [14,19]. It may address thermal boundary conditions, non-linear material stress-strain laws, finite strains, changes of static boundary conditions, temperature-dependent material properties, etc. Today, thermo-mechanical simulations are

well established in the majority of finite element codes using at least a staggered solution strategy.

Linking CFD and thermo-mechanical analysis presents a relatively new approach to tackling multi-physical problems of fire-exposed structural behavior [7,9,13,22,23]. The first linked version assumed that heat transfer from CFD to a thermal problem occurred through radiation only [17]. At the same time, Wickström coined the term Adiabatic Surface Temperature (AST) as a field which allows transferring heat fluxes composed of radiative and convective components [21,23]. Such a linking was successfully demonstrated using FDS and ANSYS codes [9,23], later extended with the Fire-thermo-mechanical interface [13].

This article shows a more versatile approach to CFD-thermo-mechanical linking using the object-oriented multi-physics integration framework abbreviated as MuPIF [3,4]. MuPIF is written in Python 3.x and defines abstract base classes for individual components, e.g. data, application, or networking. The abstract classes define generic interface in terms of provided methods. Derived classes representing particular components implement the interface. The generic interfaces allow to manipulate all the derived classes (implementing particular components) using the same generic interface. Moreover, as the simulation data are represented by objects as well, the platform is independent on particular data format(s), as the simulation data (such as microstructures, fields or properties) can be manipulated using the generic interfaces.

* Corresponding author.

E-mail addresses: stanislav.sulc@fsv.cvut.cz (S. Šulc), vit.smilauer@fsv.cvut.cz (V. Šmilauer), borek.patzak@fsv.cvut.cz (B. Patzák), kamila.cabova@fsv.cvut.cz (K. Cábová), wald@fsv.cvut.cz (F. Wald).

<https://doi.org/10.1016/j.advengsoft.2019.02.007>

Received 1 November 2018; Received in revised form 7 January 2019; Accepted 25 February 2019

0965-9978/ © 2019 Elsevier Ltd. All rights reserved.

The data exchange is based on exchange of the corresponding data components, embedding raw data and operations. This way, the models receive data with methods how to interpret the data. Therefore, the focus on services is provided by objects (object interfaces) and not on underlying data itself. In this way, the MuPIF platform is not standardizing the structure of data, it is standardizing the fundamental, core operations on the data.

The generic interfaces for applications allow to

- initialize and terminate application
- set data components as inputs
- get data components, e.g. receive the outputs from the application
- execute a single time step of a particular model

Even though the platform can be used locally on a single computer orchestrating individual applications, the real strength of the platform is its distributed design, allowing to execute simulation scenarios involving remote applications. MuPIF provides a transparent distributed object system, which takes care of the network communication between the objects when they are distributed over different machines on the network.

MuPIF has been used for linking heterogeneous commercial and in-house codes written in Fortran, C, C++, Python and Matlab, running locally or remotely over a network, simulating CFD, nonstationary thermo-mechanical tasks, phase field models for CIGS microstructure formation, light-scattering models, etc. [5].

This article describes a new API for FDS, passing an AST field in selected timesteps to the thermo-mechanical model in OOFEM [2]. Its validation on timber and concrete members proved efficient computation, robustness, and stability using built-in features from MuPIF such as field mapping algorithms and network support.

2. CFD and thermo-mechanical linking

This section reviews the used software tools and the methodology of one-way linking.

2.1. Adiabatic surface temperature

Convection and radiation present dominant boundary conditions for a structure exposed to fire. This could be facilitated by AST, a concept brought by Wickström [23]. The total heat flux to the surface of an element reads

$$q_{\text{tot}} = q_{\text{con}} + q_{\text{rad}} \quad (1)$$

Convection and radiation terms are further expressed as

$$q_{\text{con}} = h(T_{\text{g,CFD}} - T_{\text{TM}}) \quad (2)$$

$$q_{\text{rad}} = \varepsilon(R_{\text{inc,CFD}} - \sigma T_{\text{TM}}^4) \quad (3)$$

where h is the heat transfer coefficient, σ is the Stefan–Boltzmann constant, ε is the emissivity of the exposed surface, T_{TM} is the temperature of a surface in the thermal model in OOFEM, $T_{\text{g,CFD}}$ is the temperature in the CFD model in FDS and $R_{\text{inc,CFD}}$ is the so called incident radiation. It is the sum of all radiative sources in FDS

$$R_{\text{inc,CFD}} = \sum \varepsilon_i F_i \sigma T_{\text{inc},i}^4 \quad (4)$$

where $T_{\text{inc},i}$ stands for the temperature of each flame or hot surface, ε_i is its emissivity and F_i is the view factor between the source and the oriented surface of the structure. FDS can automatically obtain the value of $R_{\text{inc,CFD}}$.

FDS software computes AST, T_{AST} . It corresponds to the temperature of a perfect insulator's surface with zero conduction, see Fig. 1. The heat flux to this surface is set to zero by the following equation

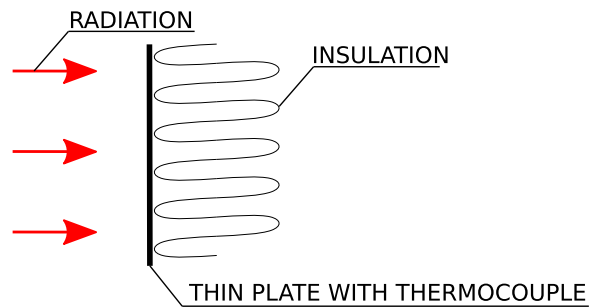


Fig. 1. Plate thermometer for AST measurement.

$$0 = \varepsilon(R_{\text{inc,CFD}} - \sigma T_{\text{AST}}^4) + h(T_{\text{g,CFD}} - T_{\text{AST}}) \quad (5)$$

The total heat flux from the fire model to the thermal model reads as

$$q_{\text{tot}} = \varepsilon(R_{\text{inc,CFD}} - \sigma T_{\text{TM}}^4) + h(T_{\text{g,CFD}} - T_{\text{TM}}) \quad (6)$$

and subtracting Eqs. (5) and (6) leads to advantageous T_{AST}

$$q_{\text{tot}} = \varepsilon\sigma(T_{\text{AST}}^4 - T_{\text{TM}}^4) + h(T_{\text{AST}} - T_{\text{TM}}) \quad (7)$$

According to Eq. (7), passing a single field T_{AST} suffices to link CFD with the thermo-mechanical task. This field is further called the AST field.

2.2. CFD task

The Fire Dynamics Simulator (FDS) [16], developed by the National Institute of Standards and Technology (NIST), is frequently used for simulating building fires. It is an open-source numerical solver written in Fortran to simulate a flow of gas during burning. FDS numerically solves a form of the Navier–Stokes equation appropriate for low-speed, thermally-driven flow with an emphasis on the transport of heat and smoke from fires. It has been used for several studies and applications in recent years, such as room fire simulation, liquid fire simulation, smoke characteristics, see a review of recent applications [1].

For the purpose of linked simulation, the FDS code version 6.5.2 has been modified in such a way that each computational time-step can be called individually and the resulting AST field obtained. Those API functions, exposed to Python, facilitate the necessary operations:

- `initASTMesh()` - initializes a MuPIF mesh and field with the coordinates of all points registered in FDS to export adiabatic surface temperatures.
- `updateASTField()` - updates all the AST values from FDS in the MuPIF field of node values on a MuPIF mesh.
- `getASTField()` - returns the MuPIF field with AST.
- `saveASTField(string filename)` - saves the field of AST into a file.
- `loadASTField(string filename)` - loads the field of AST from a file.
- `solveStep()` - solves a computational time-step with an undefined length, where FDS determines the length itself. It returns the time of the end of the time-step.

FDS needs an explicit definition of AST points of interest. They should be located slightly above an element surface so FDS knows they are in a gas phase.

FDS fortran code has been compiled as a shared library and imported to Python. Exposure of important functions to Python is realized using the `iso_c_binding` library.

2.3. Thermo-mechanical task

The thermo-mechanical analysis of structural elements takes place

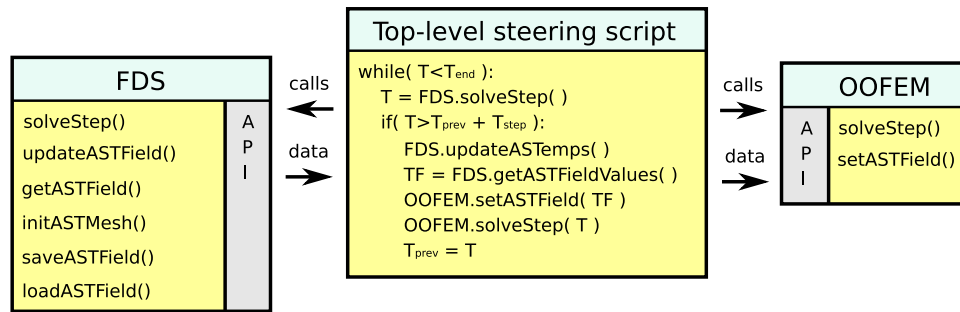


Fig. 2. API implementation for FDS and OOFEM.

in an object-oriented finite element method package called OOFEM [2]. The thermal analysis represents a general non-stationary problem with temperature-dependent material properties.

Radiative and Cauchy boundary conditions are used according to Eq. (7) with the help of the AST field. The thermal analysis passes the temperature field to the mechanical analysis, introducing thermal strain and modifying material properties such as yield strength and elastic modulus. The mechanical solution is generally non-linear.

The OOFEM code implements the BOOST [6] wrapper, which exposes important functions to Python. Particularly, the exposed functions are

- `setASTField(Field f)` - copies the values of `f` into the field of AST registered in OOFEM.
- `solveStep(double targetTime)` - solves a thermo-mechanical time step defined by the target time.

2.4. MuPIF - multi-physics integration platform

MuPIF provides an effective gluing framework between FDS and OOFEM, written in Python 3.x [3]. It offers several useful tools such as field mapping, exporting data to the VTK format, parallel computations and steering of particular models. APIs for FDS and OOFEM were developed. A top-level, steering script imports them as shared libraries, controls the execution of both codes and data synchronization, see Fig. 2.

First, FDS is called to process several computational steps until the length of our defined time-step of the thermo-mechanical task is reached. The FDS application determines its time-step itself and it is usually much shorter than the OOFEM time-step.

Once finished, the MuPIF field representation of temperature and AST fields from FDS are created. The AST field has no underlying mesh and the value in the closest point is returned. Thus, AST points need to be located close to surfaces with defined boundary conditions according to Eq. (6).

The MuPIF field of AST values is passed to OOFEM as an AST field (using `setField` method). OOFEM solves the computational step of the thermal task and passes the computed temperature field to the mechanical model. Temperature-dependent material parameters are updated. The global time step ends with computing the resulting mechanical response. Fig. 3 shows details of models and the data flow using the MODA diagram [20].

Fig. 4 shows the linking methodology. The left subfigure displays a part of the FDS mesh with a gray block for subsequent thermo-mechanical analysis. The middle subfigure zooms the block with black dots which represent AST locations. They are positioned slightly above each finite element's face exposed to fire. AST points are defined in the FDS input file, prior to computation. The right subfigure presents the temperature field which is further used for mechanical analysis. The thermal boundary conditions are evaluated in Gauss points on each

element's surface exposed to fire. Fig. 5 shows characteristic locations of AST points together with locations of the Gauss integration points. It shows that Gauss point takes temperature from the nearest AST point and integrates the contribution into power density. The FDS analysis is generally a time-consuming process and the computations can take several days. MuPIF stores temperature and AST fields at specific times to files. In this regard, it is possible to run the FDS simulation first and compute the thermo-mechanical task afterwards.

3. Validation and discussion

Validation uses two experiments with timber and concrete structures which were exposed to fire in a horizontal furnace. The testing occurred in the fire laboratory of PAVUS, a.s. The furnace inner dimensions were $4.0 \times 3.0 \times 2.57$ m (length \times width \times height). The furnace was heated by eight natural gas burners. The flue gas exhaust system used a frequency-controlled fan placed in a conduit connected to the opening 500×800 mm in the floor. In both cases, the temperature in the furnace followed the standard temperature curve [11]

$$T(t) = 345 \cdot \log\left(\frac{2}{15}t + 1\right) + 20, \quad (8)$$

where t is in seconds and T in degrees Celsius. The curve is displayed in Fig. 6 with bounds ± 100 °C according to recommendation [10].

Input parameters in the FDS analysis play a key role for accuracy. The parameters with the highest influence on AST are the material properties of furnace linings, gas fuel composition, ventilation system, calculation time step and meshing. FDS models for both simulations proved successful performance in validation.

3.1. Timber beam exposed to fire

The first validation considers glued timber beams made of spruce wood. Figs. 7 and 8 illustrate the layout of the beams in the furnace. The beams with dimensions of $120 \times 320 \times 3000$ mm were placed under the ceiling and were instrumented with coated thermocouples, see Fig. 9. High surrounding temperatures led to the burning of the beams, see Fig. 10. The experiment lasted 30 min and the initial temperature in the whole furnace was 10 °C.

The heat power of gas burners followed the curve from Fig. 11 with the maximum output of 258 kW. FDS used this curve for explicit control of the burners. Fig. 12 validates the average gas temperature.

Preliminary analysis found that the thermal conductivity of thermocouples' wiring significantly influenced the measured temperature, see Fig. 13. For this reason, only temperatures in points #1 and #2 from Fig. 9 were validated.

3.1.1. Simulation

The FDS task is composed of one global mesh consisting of $18 \times 18 \times 12$ elements and three finer meshes around the beams, each

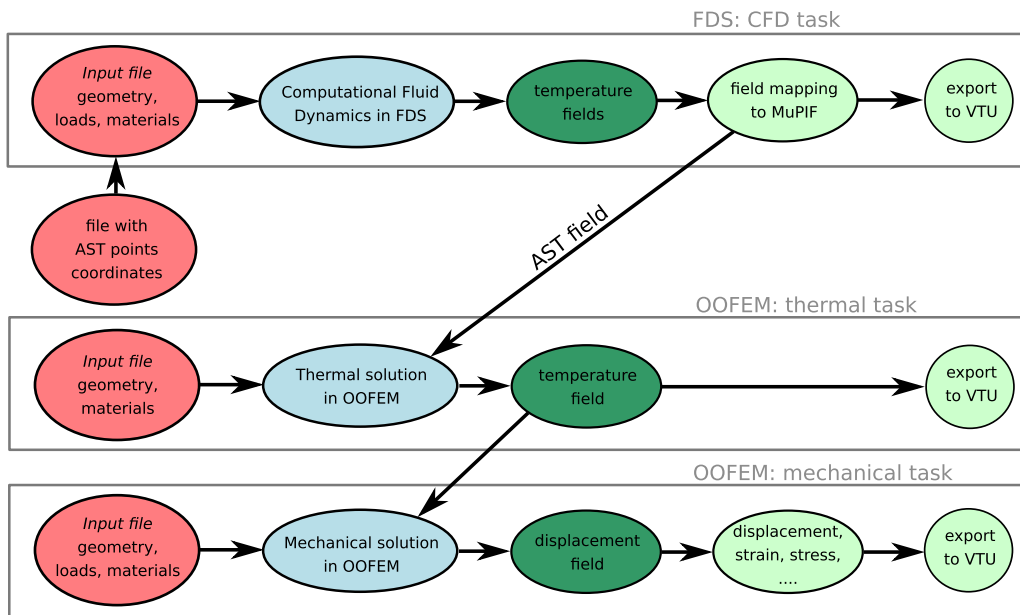


Fig. 3. Input parameters, results, data flow and output using MODA diagram, [20].

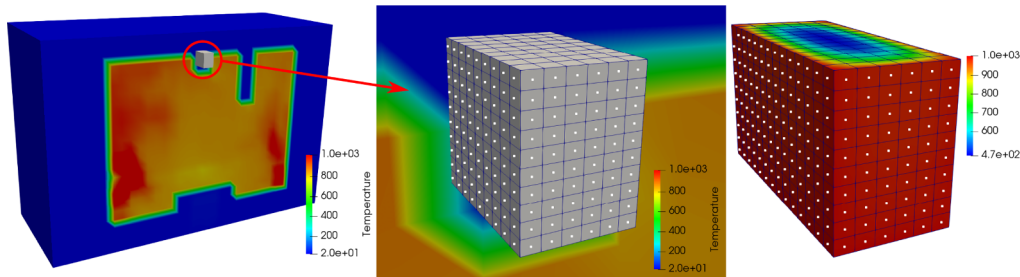


Fig. 4. Linking methodology between CFD and thermo-mechanical models. CFD temperature field (left), AST locations (middle) and block's temperature field (right).

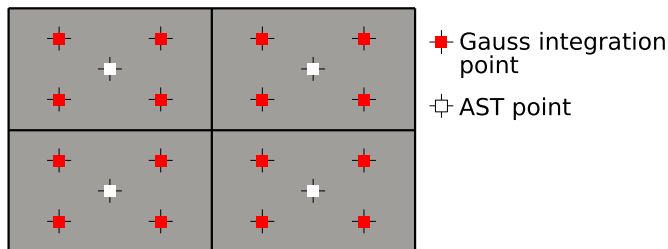


Fig. 5. Characteristic locations of AST points and Gauss integration points on four element surfaces.

consisting of $4 \times 24 \times 8$ elements, see Fig. 14. The mesh densities were designed in order to complete the computation in approximately 24 h. Fig. 15 presents the Smokeview visualization of the furnace model.

For simplicity, OOFEM considered only a 0.1 m long section of the beam. The regular mesh was composed of $24 \times 1 \times 64$ finite quadratic elements, mimicking 2D heat transport. The AST field around the beam was exported every 0.5 s, which was the time-step in OOFEM, found for good numerical stability.

Temperature-dependent wood properties followed standard curves from Eurocode 6, which describes the overall thermal behaviour. Eurocode 6 assumes that using these properties is relevant only for the first 30 min of fire exposure. More precise simulation would need

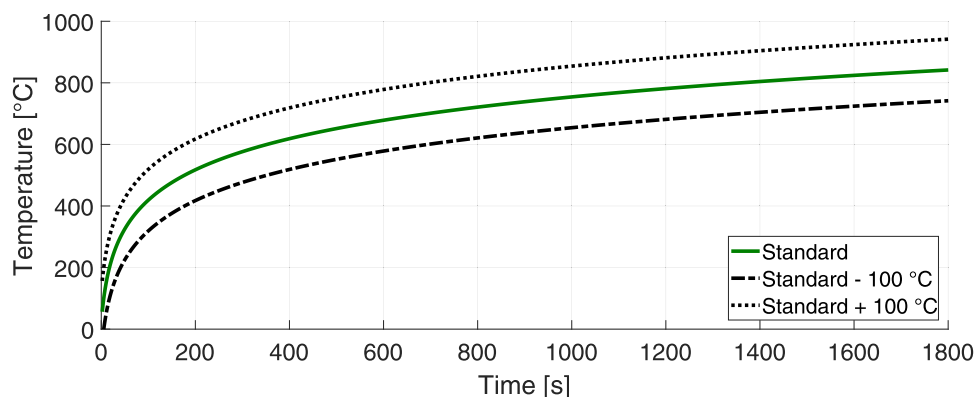


Fig. 6. Standard temperature curve with tolerances for fire resistance testing.

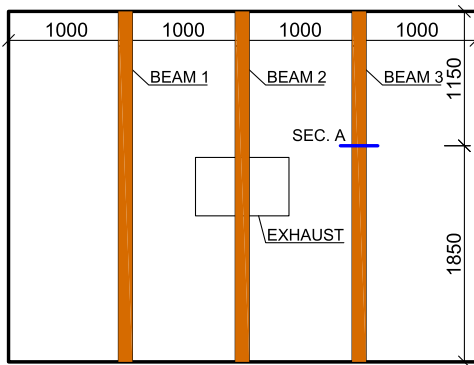


Fig. 7. Horizontal layout in the furnace.

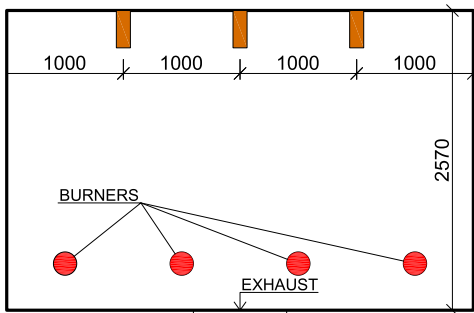


Fig. 8. Vertical layout in the furnace.

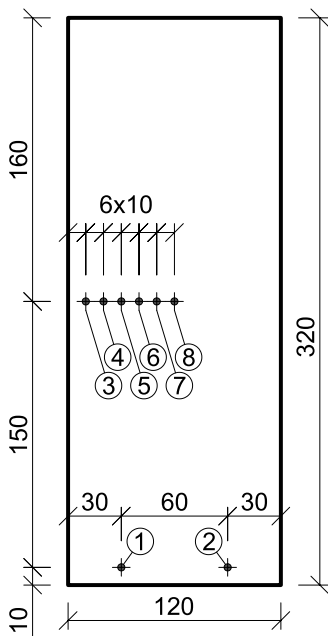


Fig. 9. Cross-section of beam 3.

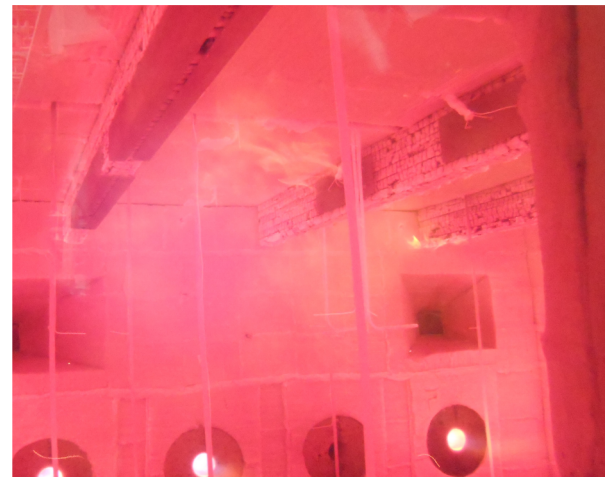


Fig. 10. Burning timber beams during the experiment at time = 1020 s.

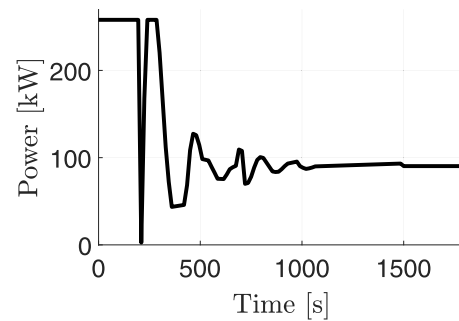


Fig. 11. Total heat power of gas burners.

3.1.2. Results and discussion

The validation of the temperature field occurred on beam #3, cross-section A and – points #1, #2, see Figs. 7 and 9. Fig. 19 shows the temperature field at 1800 s. Figs. 20 and 21 presents the results in points #1 and #2, which are less affected by wiring conductivity. The maximum absolute error yields 111.1 °C from the measured temperature range 10–757 °C, which leads to the relative error of 14.7% with regards to the maximum temperature. The reasons for these differences are i) using standard parameters instead of measuring parameters of the used material and ii) the capacity and density were modified in the interval (0, 120 °C) for better numerical stability. Considering these simplifications and the complexity of the whole simulation, the temperatures from the simulation agree reasonably well with the experiment.

The simulation also yields temperatures in points #3–#6, which are showed in Fig. 22. It points to a rapid increase of temperatures in the surface layer of finite elements (#3) compared with almost no temperature change at depth of 40 mm (#6) during the 30 min simulation, which manifests strong insulating behavior of timber. The figure also shows temperature offset due to heat diffusion into the member.

3.2. Concrete block exposed to fire

The second validation focuses on a concrete block (0.35 m × 0.15 × 0.2 m) placed below the furnace ceiling. Mineral wool insulates its top side, see Figs. 23 and 24. The experiment also involved concrete column elements, which were a part of another research project. Concrete class C30/37 with cement’s amount of 370 kg/m³ constituted the block. In order to avoid spalling of the surface, the concrete contained 1.5 kg/m³ of PP fibers. Indeed, no spalling had occurred as evident from Fig. 25.

The heat power of gas burners followed the curve from Fig. 26 with

explicit implementation of timber burnout, which is beyond the scope of this article.

Fig. 16 shows timber thermal conductivity while Fig. 17 describes timber density, assuming initial moisture content of 13.5%. Fig. 18 gives timber heat capacity with a high peak due to water evaporation around 100 °C. Those functions were partially smoothed to stabilize the numerical solution. The emissivity of the timber surface was set to 0.95, assuming a fully carbonized surface. It was found that the radiation term in Eq. (7) has the largest impact while the convection term can be neglected in this case.

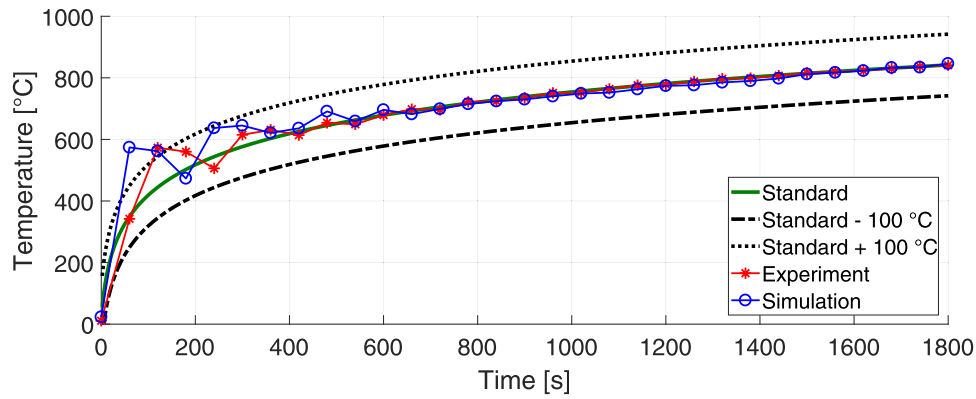


Fig. 12. Validation of average gas temperature in the furnace.



Fig. 13. Wiring to sensors.

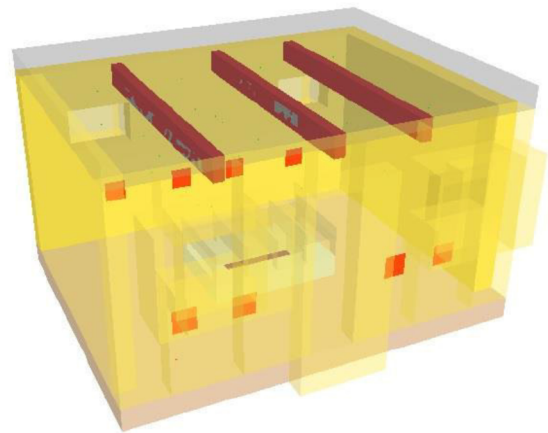


Fig. 15. FDS model depicted in SmokeView.

the maximum output of 258 kW. FDS used this curve for explicit control of the burners. Fig. 27 validates the average gas temperature. The experiment lasted 120 min and the initial temperature of the whole furnace was 10 °C.

3.2.1. Simulation

The FDS task used a global mesh consisting of $36 \times 36 \times 24$ elements, see Fig. 28. The FDS simulation took 72 hours on 4 CPU cores.

A regular mesh in OOFEM contained $14 \times 6 \times 8$ quadratic brick elements, see Fig. 29. AST sampling was 2s, corresponding with the time step of OOFEM.

Standard concrete properties followed Eurocode 2, particularly thermal conductivity displayed in Fig. 30 and heat capacity in Fig. 31.

The isotropic damage model served for demonstrating the mechanical behavior, while the damaged material stiffness tensor $K = (1 - \omega)K_e$ describes material softening. K_e is the elastic undamaged stiffness tensor and ω is the damage parameter, related to the largest previously reached equivalent strain level. We used Mazar's

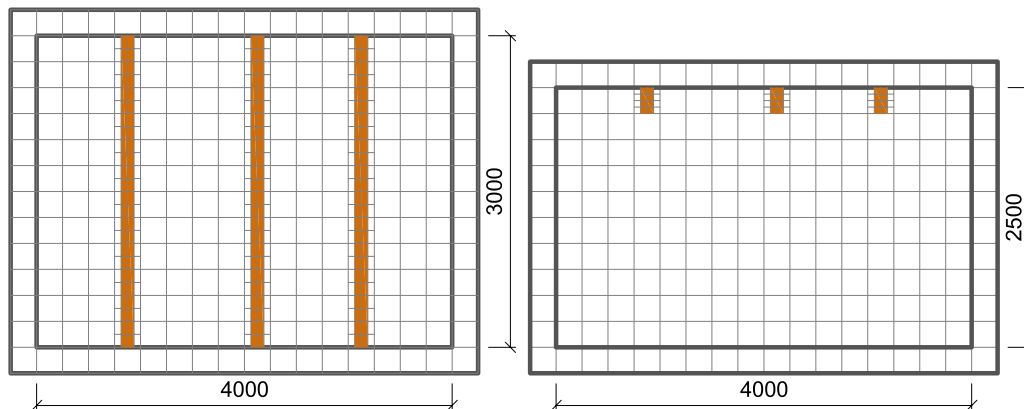


Fig. 14. Meshing in the FDS model, horizontal and vertical cut through beams.

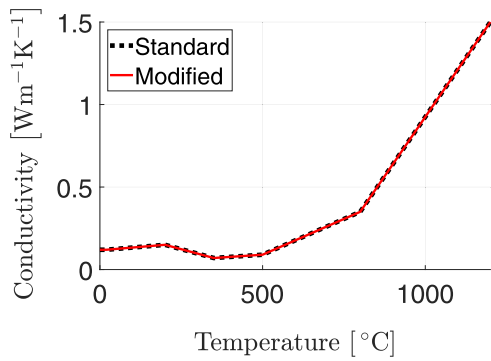


Fig. 16. Timber thermal conductivity.

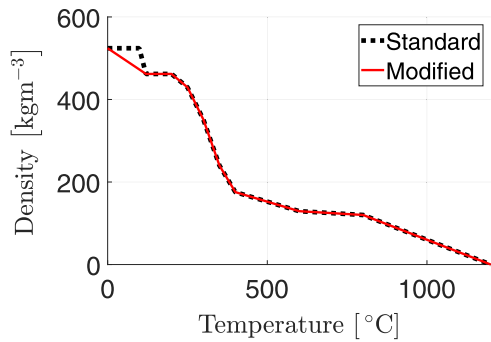


Fig. 17. Timber density.

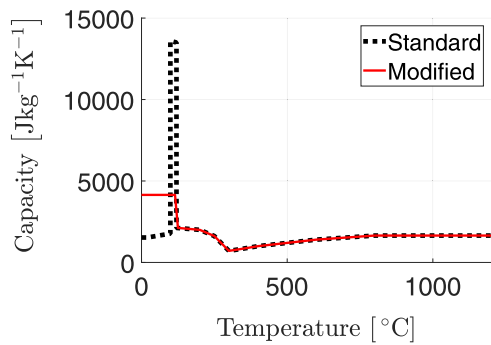


Fig. 18. Timber heat capacity.

definition, defining the equivalent strain as the sum of the maximum principal strains

$$\tilde{\epsilon} = \sqrt{\sum_{i=1}^3 \langle \epsilon_i \rangle^2} \quad (9)$$

where $\langle \epsilon_i \rangle$ are positive parts of the principal values of the strain tensor ϵ . Mechanical material properties were assumed as Young's modulus $E = 30$ GPa, density $d = 2400$ kgm⁻³, Poisson's ratio $\nu = 0.25$, coefficient of thermal expansion $\alpha = 12 \times 10^{-6}$ K⁻¹, constant tensile strength 2.1 MPa and fracture energy 250 Jm⁻². The emissivity of the concrete surface was assumed as 0.85. The heat transfer coefficient was set to zero since it has a small impact on the results, as demonstrated further in Section 3.2.3.

3.2.2. Results

Thermocouples followed the vertical line at the centre of the block, see Fig. 32. The simulation results in Figs. 33–36 present a very good match with the experimental data. There are some discrepancies, which can be caused by the assumed standard material parameters. The maximum relative error of the presented graphs is 10.4%. It occurs in

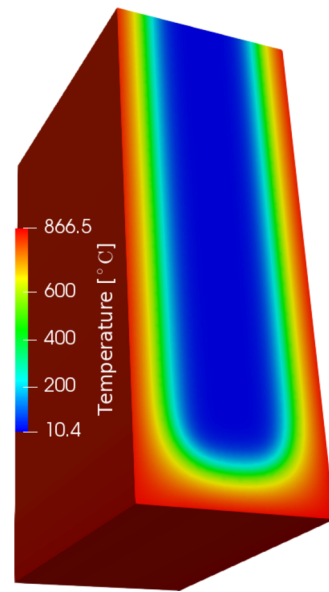


Fig. 19. Temperature in the cross-section of the beam at time $t = 1800$ s.

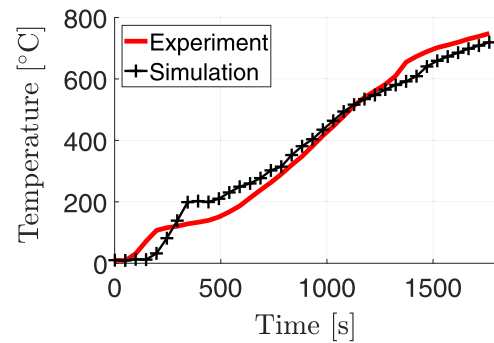


Fig. 20. Temperature in #1.

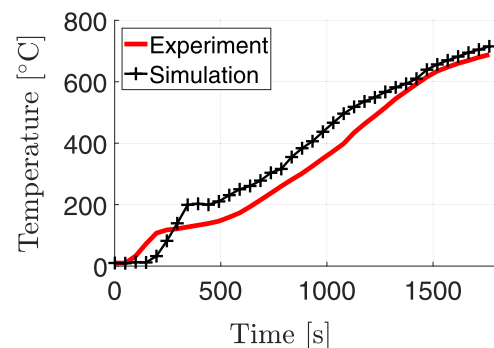


Fig. 21. Temperature in #2.

point #4 with 57.5 °C out of the maximum temperature of 554 °C.

Fig. 37 provides the visualization of the temperature field at the time of 7200 s. The mechanical task computes corresponding stresses; an example of the σ_{xx} field from the isotropic damage model is presented in Fig. 38. A corresponding scalar damage variable field is shown in Fig. 39, while Fig. 40 presents the crack width with the maximum value of 4.8×10^{-4} m. Unfortunately, the crack width remained without validation.

3.2.3. Sensitivity to heat transfer coefficient and emissivity

Eq. (7) states that the heat flow from gas to a solid is caused by radiation and convection. To elucidate the effect of both components,

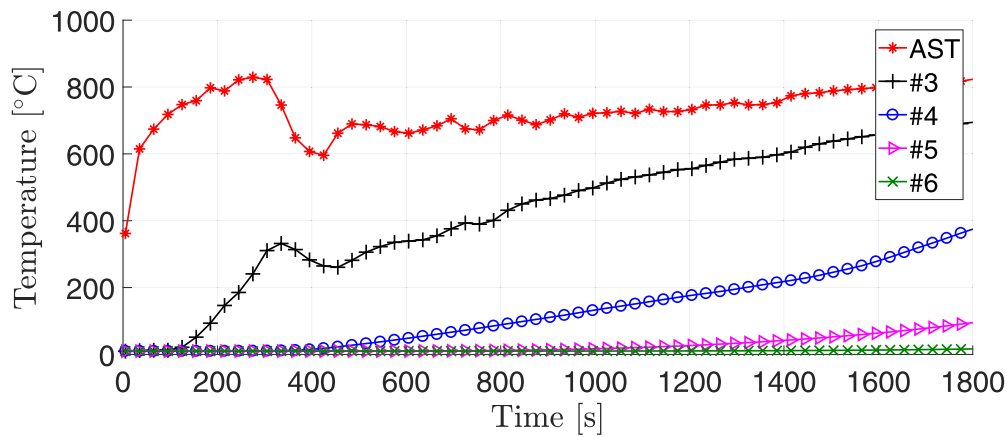


Fig. 22. Temperatures in timber member exposed to the fire.

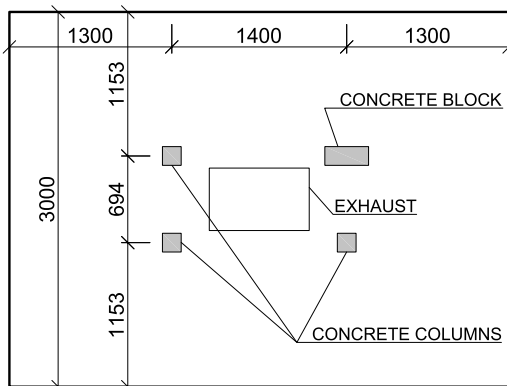


Fig. 23. Horizontal layout of the furnace.

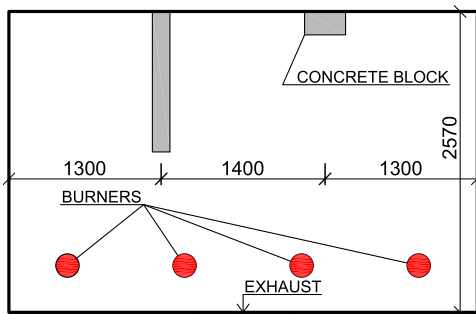


Fig. 24. Vertical layout of the furnace.



Fig. 25. Concrete block after fire exposure.

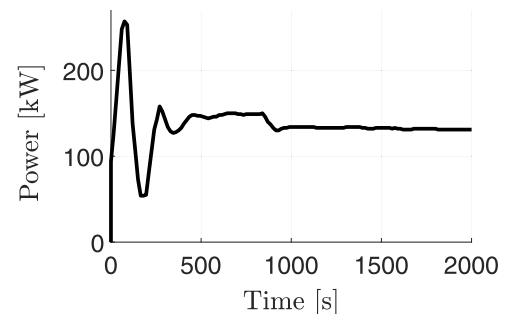


Fig. 26. Total heat power of gas burners.

the emissivity coefficient varies in the range $\epsilon \in \langle 0.85, 0.95 \rangle$ with no convection. Fig. 41 shows that the used range has little impact on the results; this is caused by the low thermal conductivity of concrete and low heat conduction decisive for internal temperatures.

The heat transfer coefficient h has little impact on temperature, see Fig. 42 with a default value of $\epsilon = 0.95$. This implies that radiation dominates the heat flow.

The default values in the simulations $h = 0 \text{ W/m}^2/\text{K}$, $\epsilon = 0.95$ for timber and for concrete made almost no difference in the results and this justifies the values which were used in the validation.

4. Conclusions

The article presents the linking of two computational codes for a complex multi-physical problem; a CFD simulation with a FDS code and a thermo-mechanical simulation using OOFEM. The approach leads to the following conclusions:

1. Adiabatic surface temperature (AST) presents a suitable and accurate concept of heat transfer between both codes, capturing radiation and convection effects.
2. MuPIF provided an effective gluing Python framework for field mapping, exporting data and orchestrating both codes. Modified FDS code with MuPIF's API is publicly available on <https://github.com/mupif/APIs> under FDS for further development.
3. Validations of the thermal response showed good accuracy for timber and concrete elements exposed to fire in a furnace. A mechanical analysis can be linked easily, as demonstrated on stress and crack state of concrete element. Computation times for presented analyses take approximately a few days.

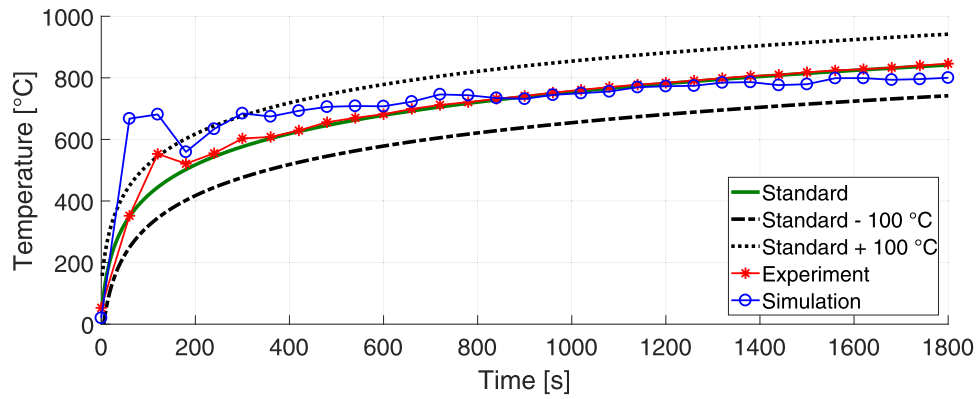


Fig. 27. Validation of average gas temperature in the furnace.

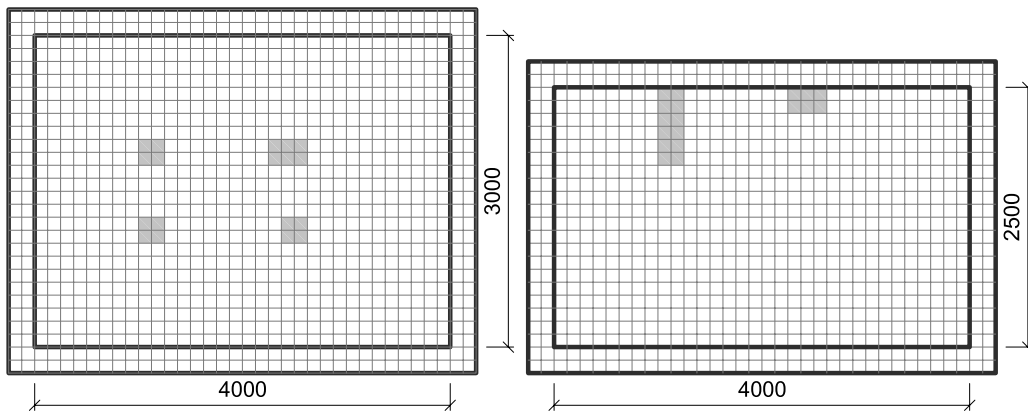


Fig. 28. Meshing in the FDS model, horizontal and vertical cut through the block.

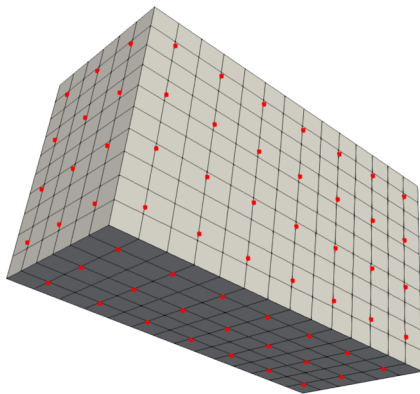


Fig. 29. OOFEM mesh with AST points.

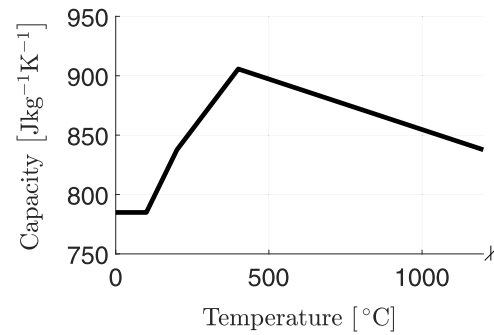


Fig. 31. Heat capacity of concrete.

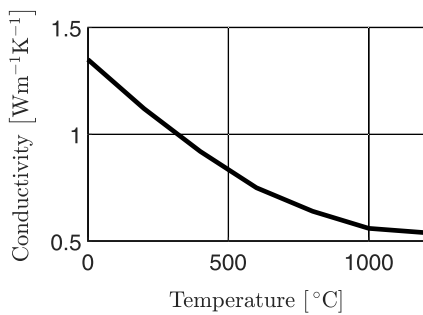


Fig. 30. Thermal conductivity of concrete.

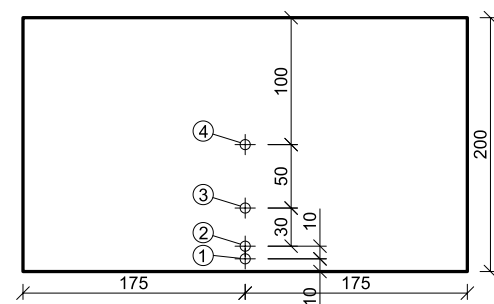


Fig. 32. Cross-section of the concrete block with positions of thermal sensors.

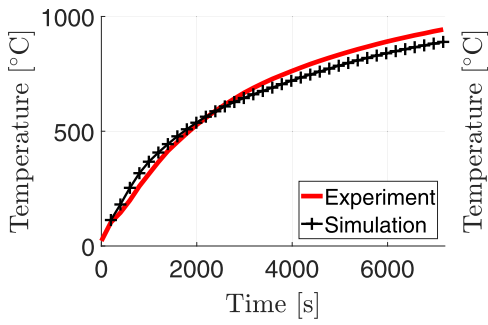


Fig. 33. Temperature in #1.

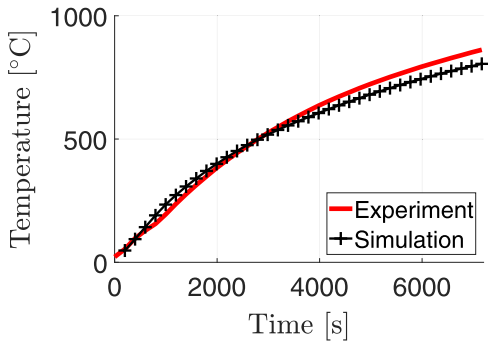


Fig. 34. Temperature in #2.

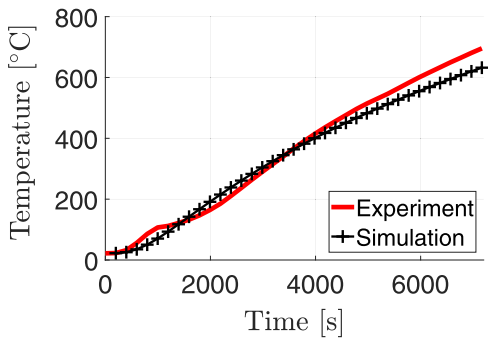


Fig. 35. Temperature in #3.

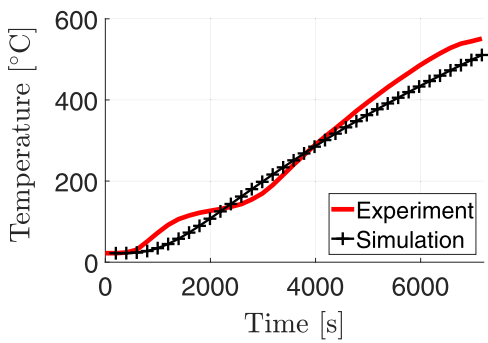


Fig. 36. Temperature in #4.

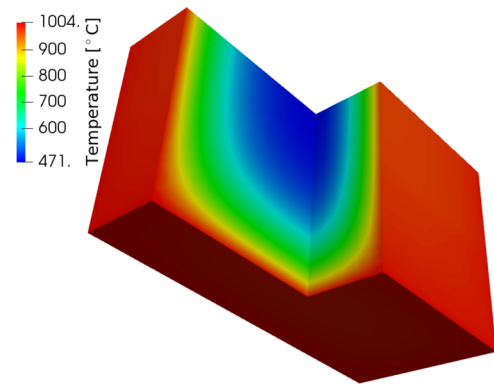


Fig. 37. Temperature at time = 7200 s.

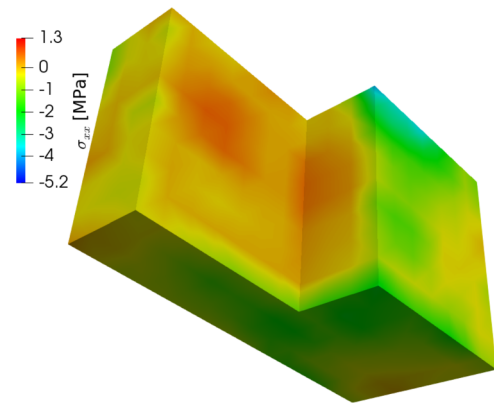


Fig. 38. Stress σ_x at time = 7200 s.

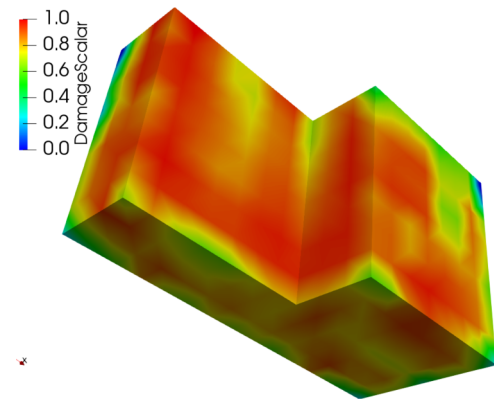


Fig. 39. Damage scalar parameter at time = 7200 s.

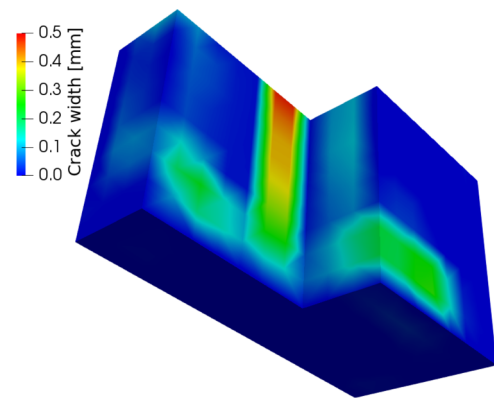


Fig. 40. Crack width at time = 7200 s.

4. Multi-physical simulation allows performing fire-safety analysis of key elements of larger structures, mechanical analysis, or approximate simulation of wood charring. Larger structures can be analyzed using the same approach, requiring for example parallel processing.

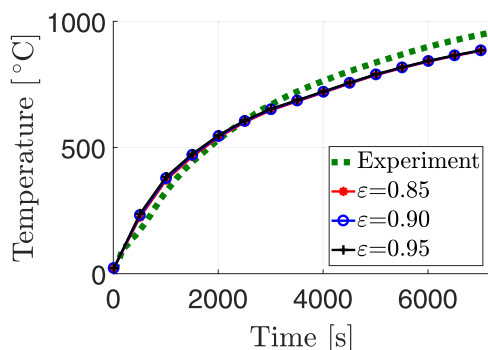


Fig. 41. Temperatures in #1 for several values of the emissivity coefficient ε with no convection.

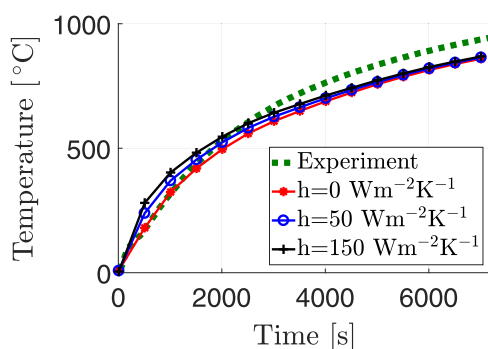


Fig. 42. Temperatures in #1 for several values of the heat transfer coefficient h with $\varepsilon = 0.95$.

Acknowledgements

We appreciate our collaborators Dr. Lukáš Blesák and Dr. Radek Štefan for their help with experiments and Martin Benýšek and Filip Zeman for FDS models. We gratefully acknowledge financial support from the Czech Science Foundation, grant 16-18448S “Coupled model of structural standard fire test”. We also gratefully acknowledge the financial support from Czech Technical University in Prague, grant number SGS19/032/OHK1/1T/11.

References

- [1] Byström A, et al. Full-scale experimental and numerical studies on compartment fire

- under low ambient temperature. *Build Environ* 2012;51:255–62. <https://doi.org/10.1016/j.buildenv.2011.11.010>.
- [2] Patzák B. OOFEM - an object-oriented simulation tool for advanced modeling of materials and structures. *Acta Polytechnica* 2012;52(6):59–66.
- [3] Patzák B, Ryppl D, Krus J. Mupif a distributed multi-physics integration tool. *Adv Eng Software* 2013;60–61:89–97. <https://doi.org/10.1016/j.advengsoft.2012.09.005>.
- [4] B. Patzák, et al. Multi-physics integration framework - mupif 2.0, 2017, <http://mupif.org>.
- [5] Patzák B, et al. Multi-physics integration framework mupif - design, operation and application to simulate cigs thin film growth for photovoltaics. *2nd international workshop on software solutions for ICME*. 2016.
- [6] Boost, <https://www.boost.org/>.
- [7] Zhang C, Li GQ, Wang R. Using adiabatic surface temperature for thermal calculation of steel members exposed to localized fires. *Int J Steel Struct* 2013;13(3):547–56. <https://doi.org/10.1007/s13296-013-3013-2>.
- [8] Duthinh D. Structural design for fire: a survey of building codes and standards. NIST Technical Note 1842. National Institute of Standards and Technology; 2014. <https://doi.org/10.6028/NIST.TN.1842>.
- [9] Duthinh D, McGrattan K, Khaskia A. Recent advances in fire-structure analysis. *Fire Saf J* 2008;43(2):161–7. <https://doi.org/10.1016/j.firesaf.2007.06.006>. <http://www.sciencedirect.com/science/article/pii/S0379711207000768>
- [10] En 1363-1 fire resistance tests - Part 1: general requirements, 2012.
- [11] En 1991-1-2: Eurocode 1: actions on structures - part 1-2: general actions - actions on structures exposed to fire, 2002.
- [12] Hadjisophocleous GV, Bénichou N. Development of performance-based codes, performance criteria and fire safety engineering methods. *Int J Eng Perform-Based Fire Codes* 2000;2(4):127–42.
- [13] Silva JCG, Landesmann A, Ribeiro FLB. Fire-thermomechanical interface model for performance-based analysis of structures exposed to fire. *Fire Saf J* 2016;83:66–78. <https://doi.org/10.1016/j.firesaf.2016.04.007>. <http://www.sciencedirect.com/science/article/pii/S0379711216300522>
- [14] Bathe KJ. *Finite element procedures*. 2nd Prentice Hall; 1995.
- [15] McGrattan K, et al. *Fire Dynamics Simulator Technical Reference Guide, Volume 3: Validation*. NIST Special Publication 1018-3, Sixth edition. National Institute of Standards and Technology; 2017. <https://doi.org/10.6028/NIST.SP.1018>.
- [16] McGrattan K, et al. *Fire Dynamics Simulator (Version 6) - User's Guide*. NIST Special Publication 1019, Sixth edition. National Institute of Standards and Technology; 2018.
- [17] Prasad K, Baum HR. Coupled fire dynamics and thermal response of complex building structures. *Proceedings of the combustion institute*. 2005. p. 2255–62.
- [18] Beata PA, Jeffers AE. Spatial homogenization algorithm for bridging disparities in scale between the fire and solid domains. *Fire Saf J* 2015;76:19–30. <https://doi.org/10.1016/j.firesaf.2015.05.008>. <http://www.sciencedirect.com/science/article/pii/S0379711215000764>
- [19] Hughes TJR. *The finite element method—linear static and dynamic finite element analysis*. Dover Publishers, New York; 2000.
- [20] The european materials modelling council - moda, homepage, <https://emmc.info/moda/>.
- [21] Wickström U. Heat transfer by radiation and convection in fire testing, fire. *Fire Mater* 2004;28:411–5.
- [22] Wickström U. *Temperature calculation in fire safety engineering*. Springer International Publishing Switzerland; 2016. ISBN 978-3-319-30170-9
- [23] Wickström U, Duthinh D, McGrattan KB. Adiabatic surface temperature for calculating heat transfer to fire exposed structures. *Proceedings of the eleventh international interflam conference*. Inter Science Communications Limited, London; 2007.